Measurement of the first and second normal stress differences in a polystyrene melt with a cone and partitioned plate tool

Author(s):
Schweizer, Thomas

Publication date:
2002

Permanent link:
https://doi.org/10.3929/ethz-b-000423035

Originally published in:
Rheologica Acta 41(4), https://doi.org/10.1007/s00397-002-0232-4

Rheol Acta (2002) 41: 337–344
DOI 10.1007/s00397-002-0232-4

ORIGINAL CONTRIBUTION

Thomas Schweizer

Measurement of the first and second normal stress differences in a polystyrene melt with a cone and partitioned plate tool

Received: 10 September 2001
Accepted: 17 January 2002
Published online: 16 April 2002

Part of this paper was presented at the Jahrestagung 2001 der Deutschen Rheologischen Gesellschaft in Berlin, 14–16 May, 2001

T. Schweizer
Institute of Polymers and
Swiss Rheocenter, ETH Zürich,
CH-8092 Zürich
E-mail: tschweiz@ifp.mat.ethz.ch

Abstract Step shear rate experiments in the range of $0.1 < \dot{\gamma} < 30s^{-1}$ ($0.14 < Wi < 42$) were performed with a PS 158K melt at 190 °C. A cone (gap angle = 0.148 rad) and partitioned plate tool was used to measure the time dependent first (N_1) and second (N_2) normal stress difference. N_1 and N_2 were extracted from a series of measurements with different ratios of R/R_{Stem}, R being the sample radius, R_{Stem} the radius of the central part of the plate connected to the transducer. A very good reproducibility was found for the measured torque. Edge fracture was observed for strains ≥18, independent of shear rate. For larger samples, the onset of edge fracture as seen by the transducer was delayed to larger strains. This is due to damping of the disturbances by the melt between the rim of the sample and the stem. The steady state value of the ratio $-N_2/N_1$ decreases from 0.24 at 0.1 s^{-1} shear rate to 0.05 at 30 s^{-1}. For $\dot{\gamma} > 10s^{-1}$ the steady state value of $-N_2/N_1$ becomes larger if smaller cone angles are used. Data for $\alpha = 0.148$ rad showed a better coincidence with the linear viscoelastic predictions of viscosity η and first normal stress coefficient $\psi_1 = N_1/\dot{\gamma}^2$ compared to smaller cones.

Keywords Polystyrene melt · First normal stress difference · Second normal stress difference · Partitioned plate · Edge fracture

Introduction

In shear flow of elastic liquids, the stress state is completely characterised by the shear stress p_{21}, the first normal stress difference $N_1 = p_{11} - p_{22}$ and the second normal stress difference $N_2 = p_{22} - p_{33}$. Whereas p_{21} and N_1 can be measured directly in a cone and plate rheometer, N_2 is not directly accessible. Nevertheless, there is a demand for second normal stress data for several reasons.

Simulations for polymer melt or solution flows through constrictions have shown that the size and shape of vortices very sensitively depend on the magnitude of N_2 (Debbaut and Dooley 1999). In order to check constitutive equations, rheological tests are chosen such that the calculated normal stresses strongly depend on assumptions made or parameters chosen in the equations. Such a test is, e.g. a reversing double step strain flow experiment (Brown and Burghardt 1995). At least in cone and plate shear flow, a direct relation was reported between a critical value of the second normal stress difference and the onset of a surface instability termed edge fracture (Lee et al. 1992; Keentok and Xue 1999). Although there is still no closed theory describing surface roughness (sharkskin) in extrusion of viscoelastic fluids, it is highly probable that this phenomenon is controlled by normal stresses. Therefore, a better knowledge of the latter quantities might help to understand and then reduce sharkskin.

There are several methods reported to determine N_2:

1. The radial distribution of the normal stress $p_{22}(r)$ in a sample in cone and plate rheometry can be directly measured by small pressure transducers flush mounted to the plate. There are few researchers who succeeded in carrying out such measurements (Christiansen and Leppard 1974; Lee et al. 1992; Magda and Baek 1994).
2. N_2 can be calculated from a combination of cone and plate and parallel plate experiments (Brown et al. 1995). The evaluation of such experiments is quite subtle because absolute values of the normal force and derivatives thereof with respect to shear rate have to be determined (see, e.g. Eggers and Schümmer 1994 for further references).
3. N_2 can be measured with optical methods in a flow birefringence experiment. Optical methods allow determining the full refractive-index tensor by directing laser-beams under different incidence angles through the flow cell. Brown et al. (1995) and Olson et al. (1998) used one tiltable probing beam and the displacement of the coupling prisms to induce flow, Kalogrianitis and van Egmond (1996) directed three probing beams through a rotating flow cell.
4. Using a cone and a partitioned plate, N_2 can be extracted by performing a series of experiments with different sample radii (Meissner et al. 1989; Eggers and Schümmer 1994; Laun 1994). Only results obtained with this method are discussed in this paper.

The number of publications on first and second normal stress differences and their negative ratio $\Psi = -N_2/N_1$ is still quite small. Table 1 summarises some of these results.

All data of *shear thinning* viscoelastic substances show that Ψ in the zero shear rate limit is in the range between 1/7 and 2/7, the limits given by the Doi-Edwards theory (Doi and Edwards 1986) without and with independent alignment approximation, respectively. Ψ seems to decrease with increasing shear rate. There is no data for melts to show this, but the calculated values of N_1 and N_2 by Debbaut and Dooley (1999) using a four mode Giesekus model clearly show this trend. For polymer solutions Magda and Baek (1994) have shown that the "shear thinning" of Ψ is the more pronounced the lower the concentration of a 4000 kg/mol PS in *n*-butylbenzene. For comparison, I would like to mention the good normal stress data for a *shear thickening* dispersion by Laun (1994). This data shows a completely different behaviour in that N_1 is negative, N_2 is positive and $N_2 \approx -0.5 N_1$.

The purpose of this paper is to show for a technical polystyrene melt how the time-dependent first and second normal stress differences can be measured in a modified cone and plate rheometer and what the experimental limitations of this method are.

Experimental

The fluid used was a melt of technical polystyrene 158K from BASF at 190 °C. Pellets were dried in a vacuum oven at 70 °C for at least 48 h. Cylindrical samples were compression moulded directly from the dried pellets using a 1 or 2 mm thick stainless steel plate with bores. The compression moulding conditions were 10 MPa for 30 min at 190 °C followed by quenching. The tablets were thoroughly deburred and stored in a vacuum oven prior to the measurement. All data in this paper is for a temperature of 190 °C.

Table 1. Measurements of the normal stress ratio $\Psi = -N_2/N_1$ reported in literature

Polymer conc. [wt%]	M_w [g/mol]	M_w/M_n	Solvent	T [°C]	Experiment	Rheometer	Normal stress measurement	Ψ (Steady state)		Source
Polyisoprene	130,000	< 1.06	none	25	Step strain	Sliding glass prisms	Birefringence	0.2–0.24		Olson et al. (1998)
Polystyrene ~8	4,000,000 (= M_v)	1.06	*n*-Butyl-benzene	25	Step shear rate	Weissenberg rheogoniometer	Flush mounted pressure transducers	0.275		Magda and Baek (1994)
Polystyrene 6	2,000,000	1.06	Tricresyl-phosphate	22	Step shear rate, shear ramp	Home built parallel plate flow cell	Birefringence	~0.28		Kalogrianitis and van Egmond (1996)
Polyisoprene 21.5	3,200,000	< 1.1	Tetra-decane	25	Step shear rate	Weissenberg rheogoniometer	Flush mounted pressure transducers	0.29		Lee et al. (1992)
LDPE 1800M BASF	146,000	11	none	150	Step shear rate	Rheometric Scientific RMS800	Normal force on partitioned plate	$\dot{\gamma}$0.5	Ψ 0.24	Meissner et al. (1989)
PS 158K	336,000	2.85	none	190	Step shear rate	Rheometric Scientific RMS800	Normal force on partitioned plate	$\dot{\gamma}$	Ψ	This work
								0.1	0.24	
								1	0.17	
								10	0.09	
								30	0.05	

The main characteristics of the test fluid are summarised in Table 1. The characteristic relaxation time λ is 1.4 s and the zero shear viscosity $\eta_0 = 44500$ Pas.

The rheometer used is a mechanical spectrometer RMS800 from Rheometric Scientific with a force rebalance transducer (maximum torque 0.2 Nm, maximum normal force 20 N). The original tools and temperature controls had to be replaced by home built ones as described by Meissner et al. (1989). The plate consists of a central stem with radius R_{Stem} connected to the transducer and an outer annulus fixed to the frame of the rheometer. In order to minimize transducer compliance effects, all tests were made using an $\alpha = 0.148$ rad cone. $R_{Stem} = 6$ mm was used for all tests at shear rates from 0.1 to 10 s^{-1}, except for one test at 10 s^{-1} with radius 9.48 mm, where $R_{Stem} = 4$ mm. All tests at 30 s^{-1} were made with the small stem.

Preheated nitrogen gas was fed into a box surrounding the tools to provide an oxygen-depleted atmosphere. For handling reasons, the stem of the partitioned plate is mounted to the transducer (top), the cone to the motor (bottom). Using a special centring tool, the dried compression moulded sample was loaded onto the cone and then squeezed between cone and partitioned plate. After reaching the measuring gap, the sample was allowed to relax for at least 10 min at 190 °C.

All sample radii R in this paper are for the molten squeezed sample. R is calculated from Eq. (1) with the sample mass m, the known density of the melt ρ (= 0.97 g/cm^3 at 190 °C), and the cone angle α:

$$R = \sqrt[3]{\frac{3m}{2\pi\rho\alpha}} \tag{1}$$

Disks with at least five different radii $R > R_{Stem}$ equally spaced on a scale $\ln(R/R_{Stem})$ were used.

Step shear rate tests were performed over a range $0.1 < \dot{\gamma} < 30 s^{-1}$ ($0.14 < Wi < 42$) for 100 shear units or until sample fracture was observed.

The shear stress p_{21} is proportional to the measured torque M acting on the stem:

$$p_{21} = \frac{3M}{2\pi R_{Stem}^3} \tag{2}$$

The shear viscosity η ($= p_{21}/\dot{\gamma}$) is shown in Fig. 1, from which the high degree of reproducibility is evident. All data is shown between 0.06 s (the time t_{adj} required by the rheometer to set a constant shear rate) and the time at which edge fracture occurred (marked by X).

The apparent normal stress N_{app} is calculated from the normal force F acting on the stem such that $N_{app} = N_1$ if $R = R_{Stem}$:

$$N_{app} = \frac{2F}{\pi R_{Stem}^2} \tag{3}$$

The following relation holds between N_1, N_2 and N_{app} (Meissner et al. 1989; Schwarzl 1990):

$$N_{app} = N_1 + 2(N_1 + 2N_2)\ln\left(\frac{R}{R_{Stem}}\right) \tag{4}$$

For $R = R_{Stem}$ it follows that $N_{app} = N_1$. In order to apply Eq. (4), one must use isochronal values of N_{app} for each R/R_{Stem} at a given strain rate. Figure 2 shows N_{app} at $\dot{\gamma} = 30 s^{-1}$ and Fig. 3 the isochronal extract at time 0.6 s. N_1 is obtained from the $\ln(R/R_{Stem}) = 0$-intercept and N_2 from the slope $2(N_1 + 2N_2)$.

In summary, out of the measured torque and normal force, three time functions result. The viscosity is proportional to the torque and $N_1(t)$ is related to the normal force of the smallest sample. The third function $N_2(t)$ is linked to the spacing of the curves in Fig. 2 and can only be obtained if measurements with different samples are made.

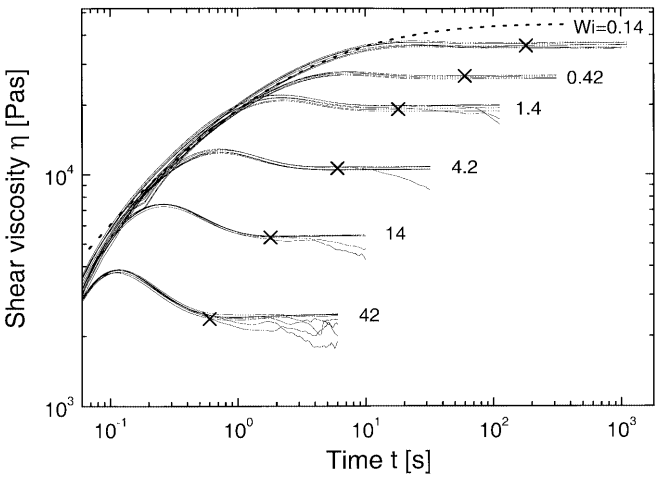

Fig. 1. Shear viscosity of PS 158 K at 190 °C measured with cone ($\alpha = 0.148$ rad) and partitioned plate ($R_{Stem} = 4$ and 6 mm). The shear rates in Weissenberg numbers are indicated in the plot. Note that each curve represents a measurement with a different ratio of R/R_{Stem}. The *X* marks a strain of 18, the minimum strain at which inhomogeneities were observed in normal force data. The *dotted line* is the linear transient shear viscosity $\eta^0(t)$ calculated from the relaxation spectrum that has been determined by shear oscillations

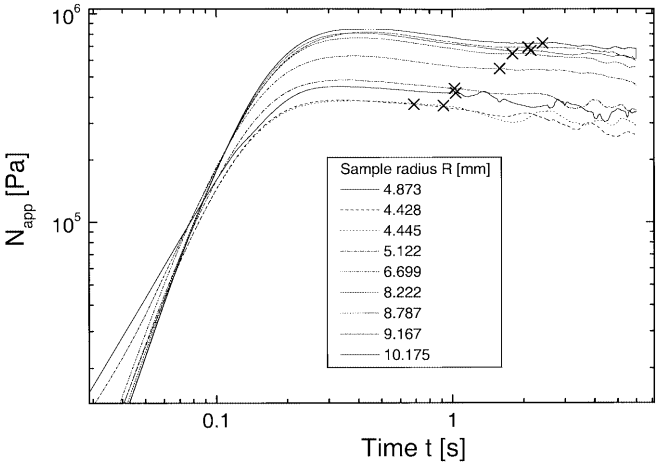

Fig. 2. Apparent normal stress $N_{app} = 2F/\pi R_{Stem}^2$ measured with cone and partitioned plate. $Wi = 42$, $R_{Stem} = 4$ mm. Sample radii R are indicated in the figures legend. The *X* marks the strain at which the data gets turbulent

The necessity to consider transducer compliance effects for normal stress measurements is well known (Hansen and Nazem 1975; Venerus and Kahvand 1994). The axial response time t_a can be estimated using the following equation:

$$t_a = \frac{6\pi R\eta}{K_a\alpha^3} \tag{5}$$

Equation (5) was derived for a modified Weissenberg Rheogoniometer with a compliant transducer. The rheometer RMS800 used in this study has a force rebalance transducer, which is non-compliant from design. However, the instrument frame stiffness of the RMS800 ($K_a = 2.4$ N/μm) is up to a factor of 10 lower than that of the Rheogoniometer used by Hansen and Nazem

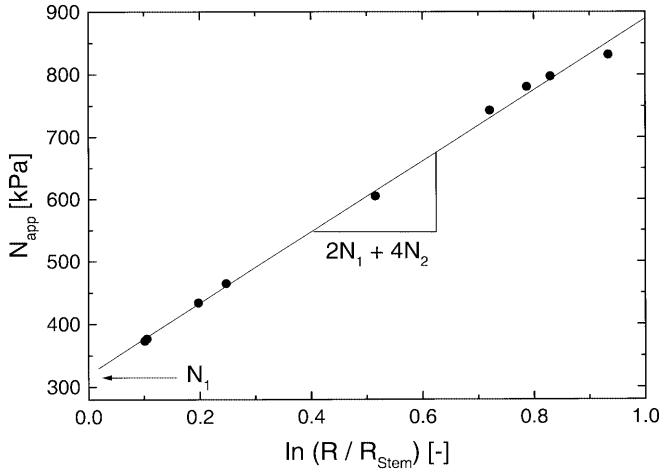

Fig. 3. Determination of the first (N_1) and second (N_2) normal stress difference from the data of Fig. 2. The data-points are isochronal values at t = 0.6 s ($\gamma = 18$). The *line* is a linear fit

($K_a = 20$ N/μm with the stiffest spring). Therefore it is justified to apply Eq. (5) also to our rheometer.

It is evident that larger cone angles α, smaller sample radii R and a stiffer construction of the rheometer lead to a shorter t_a. Transducer compliance effects can be neglected if $\lambda_a/t_a >> 1$. For the lowest and highest shear rate and the smallest and largest samples the ratio λ_a/t_a has been calculated in Table 2 for different cone angles. Here, λ_a is the shear rate dependent axial relaxation time of the melt (Carreau et al. 1997):

$$\lambda_a = \lambda \left(\frac{\eta(\dot{\gamma})}{\eta_0} \right)^{0.75} \tag{6}$$

At each shear rate, the maximum measured viscosity η_{max} has been selected for Eq. (5). The results in Table 2 show that the ratio λ_a/t_a is only close to unity for the largest cone angle. For smaller cone angles, substantial compliance effects have to be expected.

The time t_{adj} for the motor to adjust the desired deformation was determined from a series of relaxation tests (strain 10%) and has also been added to Table 2. Clearly, t_{adj} as well as t_a are strongly increasing with smaller cone angles.

Results and discussion

The primary results of this method are the first and second normal stress difference N_1 and N_2. These results, expressed as first and negative second normal stress coefficients $\Psi_1 = \frac{N_1}{\dot{\gamma}^2}$ and $-\Psi_2 = \frac{-N_2}{\dot{\gamma}^2}$ are shown for the strain rates 0.1, 0.3, 1, 3, 10, and 30 s^{-1} in Fig. 4. The latter are expressed as Weissenberg numbers $Wi = \dot{\gamma}\lambda$ with $\lambda = 1.4$ s. Figure 5 shows the equilibrium values of Ψ_1 and $-\Psi_2$ and their ratio $\Psi = -N_2/N_1$. The orientation angle χ of the macromolecules to the flow direction can be calculated from N_1 and p_{21}, using the well known relation

$$\tan(2\chi) = \frac{2p_{21}}{N_1} \tag{7}$$

This result is shown in Fig. 6. In Fig. 7, a comparison is made between the steady state values of Ψ_1 and η and the linear viscoelastic predictions calculated from the relaxation time spectrum.

Originally, two cone angles of $\alpha = 0.1$ and $\alpha = 0.148$ rad, respectively, were used to broaden the selection of radii R from a given set of compression moulded samples. However, the evaluation of the data, at a given shear rate, showed that the smaller cone yielded slightly lower values for the steady state viscosity η_{ss}, with the consequence that $N_{2,ss}(\alpha = 0.1 \text{ rad}) < N_{2,ss}(\alpha = 0.148 \text{ rad})$ and $\Psi_{ss}(\alpha = 0.1 \text{ rad}) > \Psi_{ss}(\alpha = 0.148 \text{ rad})$. This discrepancy was particularly pronounced for $\dot{\gamma} > 10 s^{-1}$. The decision on whether to use the data from the small or large cone angle was made by comparing the steady state values of Ψ_1 and η with the linear viscoelastic data in Fig. 7. The data of the smaller cone clearly showed larger deviations from these curves. Therefore, only data for the cone angle of $\alpha = 0.148$ rad is considered in this paper.

The *viscosity data* in Fig. 1 shows an excellent reproducibility. This is due to the fact that the partitioned plate tool provides a fixed and well-defined value for the radius R_{Stem}. In addition, the analysis of N_{app} (Fig. 2) showed that disturbances from the rim of the samples are strongly damped by the melt between the rim and the stem. The torque-data is already less prone to oscillations due to disturbances at the rim and damped in addition: Very smooth viscosity-data results. Viscosities in Fig. 1 falling off at the end of the test belong to small samples with radii close to the radius of the stem. The

Table 2. Axial response time t_a of transducer. PS 158K @ 190 °C, λ_a is the shear rate dependent relaxation time, rheometer axial stiffness $K_a = 2.4 \times 10^6$ N/m

Fixture	$\dot{\gamma}$[s^{-1}]	η_{max} [Pas]	α [rad]	R [mm]	λ_a [s]	t_a [s]	λ_a/t_a [-]	t_{adj} [s]
1	0.1	35,900	0.148	8.6	1.2	0.75	1.60	0.06
2	0.1	35,900	0.148	15.7	1.2	1.37	0.88	0.06
3	0.1	35,900	0.1005	8.6	1.2	2.39	0.50	0.15
4	0.1	35,900	0.1005	15.7	1.2	4.36	0.28	0.15
5	30	3,770	0.148	4.4	0.22	0.04	5.47	0.06
6	30	3,770	0.148	10.2	0.22	0.09	2.36	0.06
7	30	3,770	0.1005	4.4	0.22	0.13	1.71	0.15
8	30	3,770	0.1005	10.2	0.22	0.30	0.74	0.15
9	30	3,770	0.0777	4.4	0.22	0.28	0.79	0.25
10	30	3,770	0.0777	10.2	0.22	0.64	0.34	0.25

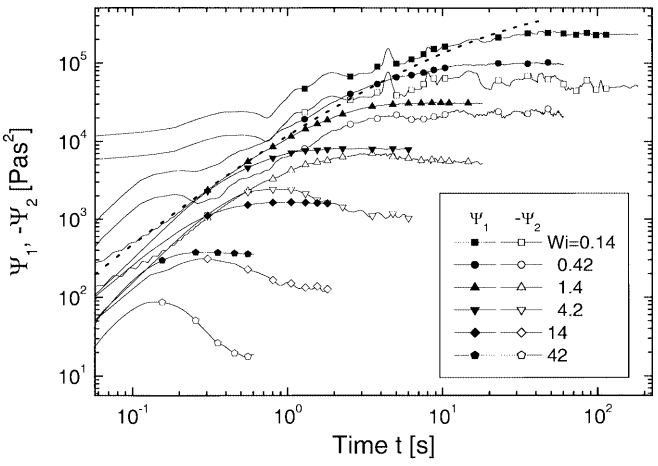

Fig. 4. First (Ψ_1) and negative second ($-\Psi_2$) normal stress coefficient. The shear rates in Weissenberg numbers are indicated in the figures legend. The data has been cut at a strain of $\gamma_{homo} = 18$. The dotted line is $\Psi_1^0(t)$

viscosities of the larger samples, which appear as straight lines, also show edge fracture. However, on zooming in, one can see that the amplitude of the disturbance is in the order of only 50–100 Pas. The overshoot η_{max}/η_{ss} is shown in Fig. 8. It is more pronounce than for N_1, but less than for $|N_2|$. If we consider shear stresses to couple to the flow on a reptation time scale and normal stresses on a Rouse time scale, then the growth of the overshoot of N_1 and η should start at Weissenberg numbers differing by $3Z = 3M_w/M_e$, with M_e being the entanglement molecular weight of the fluid (13 kg/mol, Mark 1996). For PS 158 K, $3Z \approx 75$. The dashed line in Fig. 8 is the N_1 data shifted by this factor to lower Wi. The coincidence seems good, but the overshoot at $Wi = 0.42$ is only modest for η and the shifted N_1 data.

The strain at the maximum of $\eta(t)$ is shown in Fig. 9 and has a shallow *minimum* at about $Wi = 4$. The viscosity reaches its maximum earlier than both N_1 and $|N_2|$.

When extracting steady state viscosities out of Fig. 1, it was observed that $\eta(t)$ after the overshoot in reality showed a slight positive slope. In a plot $\log(\eta)$ vs $\log(t)$ these slopes were 0.016 ± 0.002 ($Wi = 42$), 0.007 ± 0.001 ($Wi = 14$) and 0.003 ± 0.001 Pa ($Wi = 4.2$). A dependence of the slopes at constant shear rate on the radii of the samples could not be evaluated. For $Wi = 4.2$, 14 and 42 the minimum of $\eta(t)$ following the overshoot was taken as the steady state value.

The *apparent normal stress data* N_{app} was much noisier than the shear stress data. For samples with R/R_{Stem} close to unity the data showed strong oscillations as soon as edge fracture set in (see Fig. 2). For larger samples these oscillations were only visible at larger strains, because the melt between the stem and the rim substantially damped the disturbances. For this reason, the curves for $R > 6$ mm in Fig. 2 clearly show the steady state up to the X, whereas for smaller samples the steady state is masked by the disturbances from edge fracture setting in. The overshoot of N_{app} was not analysed. The strain at the maximum of N_{app} shifts to higher values with increasing sample radius. An approximate relation found is

$$\gamma(N_{app,max}) = \gamma(N_{1,max}) + 2.5\ln(R/R_{stem}) \quad (8)$$

where $\gamma(N_{1,max})$ is the strain at the maximum of N_1 as shown in Fig. 9.

The overshoot of the normal stress differences N_1 and $|N_2|$ showed a behaviour as shown in Fig. 8. $|N_2|$ shows a stronger, N_1 a weaker overshoot than η at the same Weissenberg number. The strains at the maxima of N_1

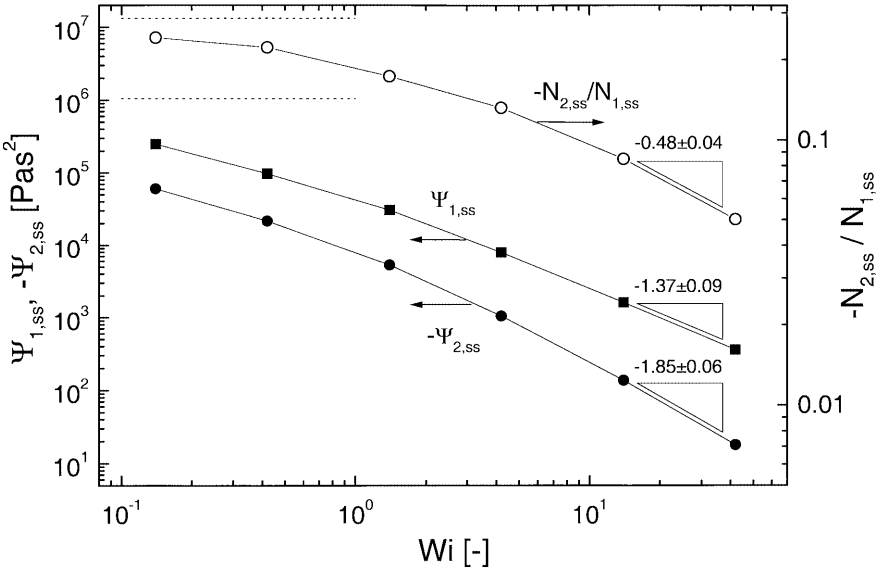

Fig. 5. Steady state values of the first (Ψ_1) and negative second ($-\Psi_2$) normal stress coefficients, and their ratio ($-\Psi_{2,ss}/\Psi_{1,ss} = -N_{2,ss}/N_{1,ss}$). The *dotted lines* represent the 2/7 limit of $-N_2/N_1$ from the Doi-Edward theory and the 1/7 limit if the independent alignment approximation is dropped (Larson 1998). The *triangles* indicate the approximate slope of the curves at high Weissenberg numbers. The Doi-Edward predictions for these slopes are for Ψ_1: –2, $-\Psi_2$: –2.5 and for $-N_2/N_1$: –0.5 (Kalogrianitis and van Egmond 1996)

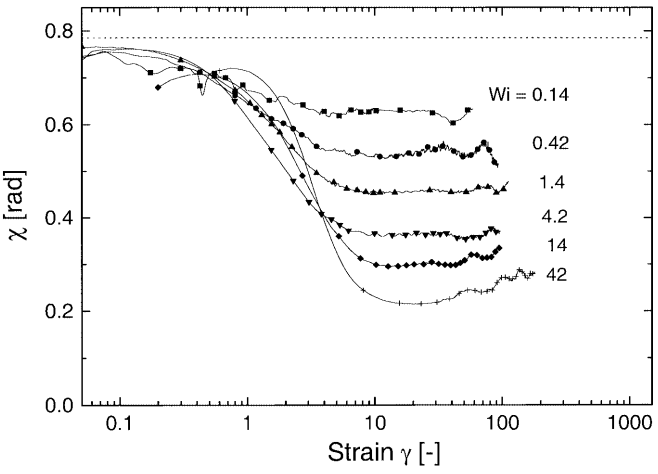

Fig. 6. Orientation angle χ (Eq. 7) vs strain. The shear rates in Weissenberg numbers are indicated in the figures legend. $\gamma = 18$ is the minimum strain at which turbulences are seen in the normal force data. The *dotted line* is the equilibrium value of χ (45°)

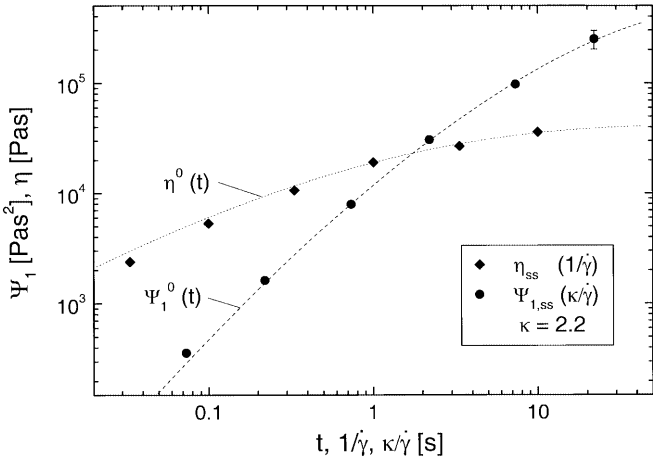

Fig. 7. Steady state values of η and Ψ_1. The *dotted and dashed lines* are the linear viscoelastic predictions $\eta^0(t)$ and $\Psi_1{}^0(t)$, respectively, calculated from the relaxation time spectrum. The Gleissle mirror relations (Gleissle 1980) were applied to $\eta_{ss}(\dot{\gamma})$ and $\Psi_{1,ss}(\dot{\gamma})$ with a factor of $\kappa = 2.2$ to get $\eta_{ss}(1/\dot{\gamma})$ and $\Psi_{1,ss}(\kappa/\dot{\gamma})$. The size of the symbols corresponds to the error-bars

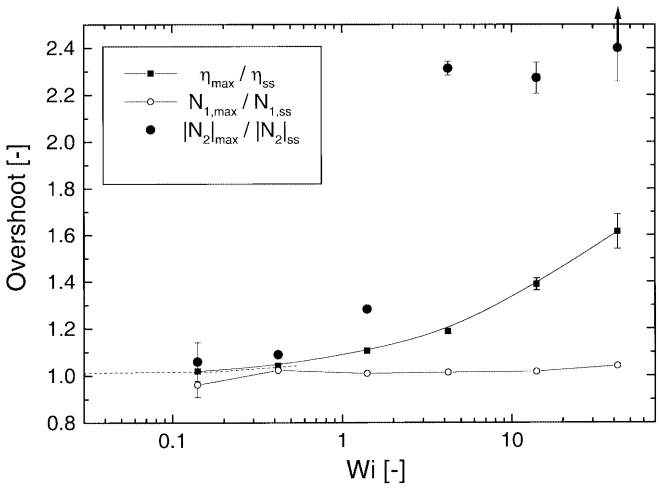

Fig. 8. Ratio of the maximum to the steady state value (overshoot) of η, N_1 and $|N_2|$. For the *symbols without error-bars*, the error is in the order of the size of the symbols. The *dotted line* is the N_1-data shifted by a factor of 75 to smaller Weissenberg numbers. The N_2-data with the *arrow* is outside of the picture at an overshoot of 4.84

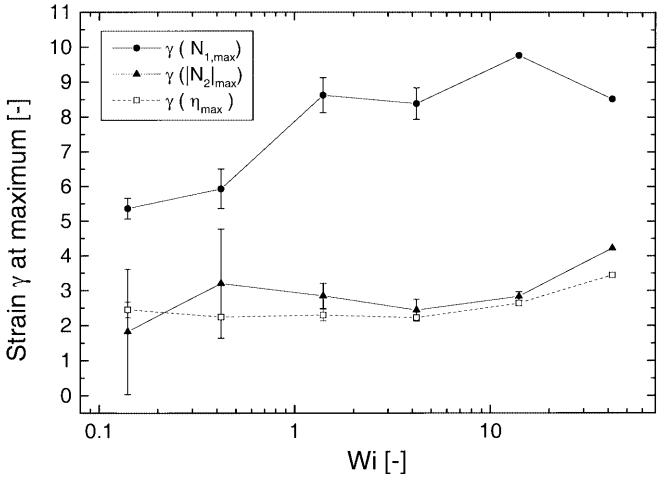

Fig. 9. Strain γ at the maxima of η, N_1 and $|N_2|$. For the *symbols without error-bars*, the error is in the order of the size of the symbols

and $|N_2|$ in Fig. 9 show an interesting behaviour. Whereas $\gamma(|N_2|_{max})$ has a shallow *minimum* at about the same Weissenberg number as η, $\gamma(N_{1,max})$ shows values shifted to larger strains and with the *maximum* at about six Weissenberg numbers.

Figure 6 shows that the macromolecules reach their maximum orientation to the flow within a few shear units. However, even at the highest Weissenberg number of 42, the molecules still keep an angle χ of 12° to the flow direction. This shows that due to the strong disentanglement leading to shear thinning, the macroscopic flow loses more and more grip to turn the molecules closer to the direction of the flow.

The minimum orientation χ_{min} is reached between a strain of about 5 (Wi = 0.14) and 20 (Wi = 42). Almost no undershoot is observed. It is interesting to note that *edge fracture is only observed* at a minimum strain of 18, i.e. when the *molecules have reached their steady state orientation*.

An experiment was terminated when either the normal force was too high or by edge fracture.

For example, for the melt of the technical polystyrene 158 K at 190 °C, the maximum *normal force* of 20 N was reached at a strain rate of 30 s^{-1} with a sample of 10 mm melt radius. These values hold for $R_{Stem} = 4$ mm and $\alpha = 0.148$ rad.

Edge fracture has been studied by analysing the time dependence of N_{app} (Fig. 2) and is manifested as oscillations or as a sudden increase or decrease of the normal force signal. Since the melt between the rim and the stem damps the disturbance, edge fracture at the rim of the sample is only registered by the transducer with a time delay. The strain at which such a disturbance is first seen in the N_{app}-data shall be denominated γ_{homo}. Analysing γ_{homo} for the shear rates 0.1, 0.3, 1, 3, 10, and 30 s^{-1} resulted in an approximate relation:

$$\gamma_{homo} = 18 + 10\ln(R/R_{stem})\dot{\gamma}^{0.5} \quad (9)$$

There is a minimum strain of about 18 below which no inhomogeneous flow was observed, independent of shear rate. At $\dot{\gamma} = 30s^{-1}$ it takes 0.6 s to reach $\gamma_{homo} = 18$. One might argue that steady state data reported for this shear rate is not really equilibrium data since $\lambda = 1.4$ s. However, one has to consider that the linear viscoelastic relaxation time λ ($= \eta_0 J_{e0}$) is also subjected to shear thinning. Using the ansatz sited by Carreau et al. (1997), Eq. (6), λ_a has to be used for discussion. Table 2 provides $\lambda_a = 0.22$ s for $\dot{\gamma} = 30s^{-1}$ and this is well below 0.6 s.

It is generally accepted in the literature that a critical value of the second normal stress difference $-N_{2,crit}$ is the parameter governing the onset of *edge fracture* (see, e.g. Magda and Baek 1994):

$$-N_{2,crit} = \frac{K\Gamma}{R\alpha} \quad (10)$$

with Γ the surface tension of the melt and K a material independent constant depending on temperature and shear rate. Equation (10) predicts that at constant shear rate and cone angle, $|N_2|_{crit}$ will decrease with increasing sample radius. This means that larger samples should fracture at smaller strains. Our results, however, show that this is not the case.

What is the reason for this discrepancy? Usually, authors dealing with Eq. (10) visually observe the rim of the sample to decide when the critical strain γ_{homo} is reached. In our case, only the transducer signal was considered. Tests at $\dot{\gamma} = 10s^{-1}$ and $\alpha = 0.1005$ rad have clearly shown that for the same sample radius R, γ_{homo} as well as $\gamma(N_{app,max})$ of N_{app} are clearly shifted to higher strains when using $R_{Stem} = 4$ mm instead of 6 mm. This implies that there is a time delay between the event "edge fracture occurring at the sample rim" and the same event being seen by the transducer. This time delay is the larger the larger the ratio R/R_{Stem}. The tenor of this is that values of γ_{homo} and γ_{max} reported here cannot unrestrictedly be compared with data from visual observations of the rim.

The measured values of $|N_2|_{crit} = -N_2\big|_{\gamma_{homo}=18}$ are shown in Fig. 10. From these, the constant K was calculated using Eq. (10). The radius of the stem is used for R, with an assumed uncertainty of 1 mm to calculate the error bar. Γ was set as 28.5 mN/m (Mark 1996). The material independence of K cannot be checked with the data of this work.

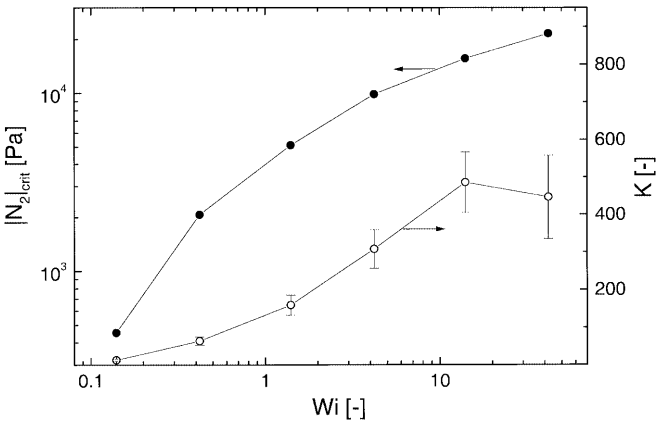

Fig. 10. Critical value of the second normal stress difference $|N_2|_{crit}$. These data are taken from Fig. 4 at the strain $\gamma_{homo} = 18$. The error-bars are in the order of the size of the symbols. The constant K in Eq. (10) is calculated from this data

Drawbacks

The cone and partitioned plate tool used for the measurements is quite delicate in handling. The fixed annulus of the plate has to be well centred to leave a gap of 0.1 mm to the stem connected to the transducer. The gap has to be thoroughly cleaned after each test.

To obtain the time-dependent first (N_1) and second (N_2) normal stress differences at one shear rate, at least five tests have to be performed with different sample radii. Thus, if only N_1 is needed, this method is much more time-consuming than a measurement of N_1 with a conventional cone and plate tool. In addition, the large amount of material required can be a problem when dealing with expensive special polymers.

Equation (9) shows that larger samples shift the end of the homogeneous flow γ_{homo} to larger strains. This should be an advantage from the experimental point of view. However, the isochronal evaluation of Eq. (4) requires that samples with different radii be used. The largest strain γ_{limit} at which Eq. (4) can be evaluated is given by γ_{homo} of the smallest sample. Thus, the closer R of this sample is to R_{Stem}, the closer γ_{limit} is to 18 (see Eq. 9). A large part of good data of the other samples (see, e.g. data for $R > 6$ mm in Fig. 2) cannot be used. If R of the smallest sample is increased, γ_{limit} can be increased as well. However, since the evaluation of Eq. (4) involves an extrapolation of the data to $\ln(R/R_{Stem}) = 0$, the latter process becomes more erroneous and the quality of the data drops.

Conclusions

The method presented here is a simple way to determine the first and the second normal stress difference in a sense that only step shear rate tests with one tool have to be performed. However, since measurements with different radii have to be made, the demand for sample preparation time, measurement time and material required is high.

The time delay between edge fracture occurring at the rim and being seen by the transducer is an interesting feature of this method. Whether the rheology will somehow be influenced by this delay cannot be discussed here but needs comparison with other methods or simulations. The time delay could be one reason for the poor transient behaviour at the beginning of the tests. Moreover, λ_a/t_a (Eqs. 5 and 6 and Table 2) is close to 1 for the fluid used. Therefore, transducer compliance effects might come into play at the beginning of the tests.

Earlier tests with different cone angles α have shown that at $\dot{\gamma} > 10s^{-1}$, the response of the melt strongly depends on α. Consequently, only one large cone angle (0.148 rad) has been used to acquire the data presented here. The strong dependence of normal force response on cone angle is, by the way, a long known fact (Meissner 1972).

Non-linear transient shear measurements not only require a careful selection of the cone angle, but are also subjected to limitations due to the maximum normal force of the rheometers. The 20 N of the rigid steel-frame RMS800 are based on the rheological knowledge of the 1980s and allow for reproducible, reliable measurements in that range. Today, rheometers for 50 N normal force can be bought, but they have compliant aluminium housings...

Acknowledgments The author would like to thank Marina Karlina and Jürg Hostettler for accurately performing the normal force measurements. Thorough discussions with Dave Venerus helped to shape this paper in a more accurate way. Prof. Meissner is thanked for his always kind and helpful advice out of his large box of experience. For financial support, the author would like to thank the Swiss Rheocenter at the ETH Zürich, Switzerland.

References

Brown EF, Burghardt WR (1995) First and second normal stress difference relaxation in reversing double-step strain flows. J Rheol 40(1):37–54

Brown EF, Burghardt WR, Kahvand H, Venerus DC (1995) Comparison of optical and mechanical measurements of second normal stress difference relaxation following step strain. Rheol Acta 34:221–234

Carreau JP, de Kee DCR, Chhabra RP (1997) Rheology of polymeric systems. Hanser Publishers, Munich

Christiansen EB, Leppard WR (1974) Steady-state and oscillatory flow properties of polymer solutions. Trans Soc Rheol 18:65–86

Debbaut B, Dooley J (1999) Secondary motions in straight and tapered channels: Experiments and three-dimension finite element simulation with a multimode differential viscoelastic model. J Rheol 43(6):1525–1545

Doi M, Edward SF (1986) The theory of polymer dynamics. International series of monographs on physics 73, Oxford

Eggers H, Schümmer P (1994) A new method for determination of normal-stress differences in highly visco-elastic substances using a modified Weissenberg rheometer. J Rheol 38(4):1169–1177

Gleissle W (1980) Rheology. 2. Fluids. Astarita G, Marrucci G (eds) Plenum Press, New York (Proceedings of the VIIIth International Congress on Rheology, Naples, Sept 1–5, 1980)

Hansen MG, Nazem F (1975) Transient normal force transducer response in a modified Weissenberg Rheogoniometer. Trans Soc Rheol 19(1):21–36

Kalogrianitis SG, van Egmond JW (1996) Full tensor optical rheometry of polymer fluids. J Rheol 41(2):343–364

Keentok M, Xue SC (1999) Edge fracture in cone-plate and parallel-plate flows. Rheol Acta 38:321–348

Larson RG (1998) The structure and rheology of complex fluids. Oxford University Press, Oxford

Laun HM (1994) Normal stresses in extremely shear thickening polymer dispersions. J Non-Newtonian Fluid Mech 54:87–108

Lee CS, Tripp BC, Magda JJ (1992) Does N_1 or N_2 control the onset of edge fracture? Rheol Acta 31:306–308

Magda JJ, Baek SG (1994) Concentrated entangled and semidilute entangled polystyrene solutions and the second normal stress difference. Polymer 35(6):1187–1194

Mark JE (1996) Physical properties of polymers handbook. AIP Press, Woodbury, New York

Meissner J (1972) Modification of the Weissenberg Rheogoniometer for measurement of transient rheological properties of molten polyethylene under shear. J Appl Polym Sci 16:2877–2899

Meissner J, Garbella RW, Hostettler J (1989) Measuring normal stress differences in polymer melt shear flow. J Rheol 33(6):843–864

Olson DJ, Brown EF, Burghardt WR (1998) Second normal stress difference relaxation in a linear polymer melt following step-strain. J Polym Sci: Part B: Polym Phys 36:2671–2675

Schwarzl FR (1990) Polymermechanik. Springer, Berlin Heidelberg New York

Venerus DC, Kahvand H (1994) Normal stress relaxation in reversing double-step strain flows. J Rheol 38(5):1297–1315